Fast Beam Discovery and Adaptive Transmission Under Frequency Selective Attenuations in Sub-Terahertz Bands

Junliang Ye, *Member, IEEE*, Hamid Gharavi, *Life Fellow, IEEE*, and Bin Hu, *Senior Member, IEEE*

***Abstract*—Sub-THz-based communication needsultra-large antenna arrays to generate pencil-like beams under the stringent requirements of line-of-sight (LoS) to overcome the effect of the rapid attenuation of signal strength, including atmospheric attenuation. In addition, the complexity of attaining narrower beamwidth, whichalsorequires fast and perfect alignment between the TX-RX pair, makes the sector sweeping-based beam discovery approach no longer suitable. To solve these challenging problems, in this paper we propose a leaky waveguide (LWG)-assisted, high-resolution codebook-based beam discovery, precoding, and combining schemetogether with an adaptive frequency hopping spread spectrum (FHSS) for a network with relays and small base stations (SBS). The proposed method can help the transmitter quickly determine a suitable beam pattern for an LoS path requiring only limited feedback information. In the beam discovery phase, we use LWG to attain valuable information about the angle of departure (AoD) and angle of arrival (AoA). LWG has also been used to identify frequency selective attenuated regions, which can change from time to time depending on the local atmospheric moisture conditions. To mitigate the impact of such attenuations, we opt for an adaptive Frequency Hopping Spread Spectrum (FHSS). The simulation results indicate that our beam discovery and FHSS based method can achieve a much higher performance thanbaseline methods.**

***Index Terms*—Sub-THz, relay, leaky wave guide, beam discovery.**

I. Introduction

WITH the rapid growth in wireless traffic and the continuing trendstoward faster data communications, the next generation wireless standard is anticipated to move further towards higher frequency bands [1]. Sub terahertz (sub-THz) communications and massive multiple input multiple output (massive MIMO) are two key technologies that can support the extreme performance requirements beyond 5th generation cellular networks (B5G) [2]. Thanks to the recent development of semiconductor technology, widely tunable sub-THz generators can transmit broadband signals at room temperature [3], [4]. However, compared with the sub-6 GHz and sub-100 GHz spectrum, transmissions on the sub-THz bands suffer from higher path loss, higher system complexity, and frequency selective atmospheric attenuations [5]. Therefore, new technologies for communications on the sub-THz spectrum need to be investigated to overcome these challenges [6].

In order to compensate for the higher path loss during signal transmission on the sub-THz spectrum, transmitters are required to be equipped with larger antenna arrays [7]. Recently there has been a growing interest in massive MIMO with hybrid precoding for THz and sub-THz communications [8], [9], [10], [11], [12], [13], [14], [15], [16], [17], [18], [19], [20], [21]. For instance, a series of technologies, such as THz signal generation, modulation, and radiation methods, including the development of channel models, noise, and hardware-impairment, have been studied in [8]. Three representative THz precoding techniques, i.e., analog beamforming, hybrid precoding, anda delay-phase precoding, have also been investigated in terms of different structures and designs [9]. The authors of [10] propose a switches-assisted dynamic array-of-subarrays hybrid precoding architecture to reduce the power consumption while meeting the data rate requirement in THz ultra-massive MIMO systems. To compensate for the array gain loss caused by beam splitting, the authors of [11] introduce a new hybrid precoding architecture called delay-phase precoding (DPP). To solve the beam splitting problem in the proposed DPP, an additional time delay network is connected to the phase shifters, which converts phase-controlled analog precoding into a delay-phase controlled analog precoding. In [12] two new sparse radio frequency (RF) chain antenna structures, including fully connected and subarray, are designed for wideband THz massive MIMO orthogonal frequency division multiplexing (OFDM) systems with beam squint. Moreover, the authors of [12] formulate an average rate maximization problem by jointly designing hybrid analog/digital precoding at the transmitter and analog combining algorithm at the receiver. In this work, they also evaluate the performance of a candidate B5G scenario with THz-enabled massive MIMO access points mounted on street lampposts to servepedestrian. Furthermore, in [13] the authors use spectral efficiency (SE) and energy efficiency (EE) as the metrics to assess the performance of three precoding schemes; namely analog-only beamforming, hybrid precoding with baseband zero-forcing, and singular value decomposition precoding. To

Manuscript received 28 March 2022; revised 13 October 2022; accepted 28 December 2022. Date of publication 6 February 2023; date of current version 20 March 2023. The associate editor coordinating the review of this manuscript and approving it for publication was Dr. Weiyu Xu. *(Corresponding author: Junliang Ye.)*

The authors are with the National Institute of Standards and Technology, Gaithersburg, MD 20899 USA (e-mail: junliang.ye@nist.gov; hamid.gharavi@nist.gov; bin.hu@nist.gov).

Digital Object Identifier 10.1109/TSP.2023.3236166

analyze the best beam steering direction, [14] uses a closed-form expression to find the lower-bound of the achievable rate in a large subarray antenna regime.

A single carrier minimum mean square error (MMSE) precoding and detection algorithm for frequency selective THz channels is proposed in [15]. Furthermore, the sparsity property of the channel is utilized to reduce the complexity of the proposed algorithm [15]. To enable massive connections in THz micro-scale networks, the authors of [16] offer a novel hybrid beamforming (BF) scheme with distance-aware multi-carrier (DAMC) modulation and beam division multiple access (BDMA). In their approach an iterative power allocation strategy is designed to maximize the achievable sum-rate of the network. The maximization of the energy efficiency (EE) problem in THz non-orthogonal multiple access (NOMA) MIMO systems is investigated by the authors in [17] where the original optimization problem is divided into user clustering, hybrid precoding, and power optimization. Then, to enable fast convergence, they utilize an enhanced K-means machine learning algorithm. Using a realistic power consumption model, the performance of the generalized hybrid precoding array structure in a cellular assisted vehicular communication scenario is investigated in [18]. A novel wideband hybrid beamforming scheme with two digital beamformers is proposed by the authors in [19]. Considering an imperfect channel state information (CSI), they offer a probabilistic robust hybrid beamforming scheme to combat channel estimation errors. In [20] two multi-resolution time-delay codebooks are designed for a subarray hybrid precoding structure. Based on the proposed codebooks, a hierarchical beamforming training strategy with reduced overhead is then proposed to enable simultaneous training for multiple users.

While the aforementioned studies reveal substantial progress in massive MIMO assisted THz and sub-THz communications, the challenge is how to design a reliable high-speed network that can compensate the effect of rapid signal attenuation as the distance between transmitters and receivers increases. Based on the analysis in [22], when the transmission distance exceeds one meter, the signal transmitted at 300 GHz frequency will suffer from a 70 dB path loss. Furthermore, transmissions on the THz or sub-THz spectrum depend heavily on the availability of a line-of-sight (LoS) path between the transmitters and receivers. Recently, there has been a growing number of publicationsfocused ona new network architecture that can support longer-range, non-line-of-sight (NLoS) communications [23], [24], [25], [26], [27], [28], [29], [30], [31]. For example, [23] introduces a network with both THz and sub-6 GHz transmissions where the latter is used to supplement the shortcomings of THz transmissions. In [24], hypersurfaces are considered to control the propagation characteristics of THz communications in order to improve the transmission distance and solve NLoS problems. Similar to hypersurfaces, intelligent reflecting surfaces (IRS), which can smartly reconfigure the propagation environment,studied in [25]. In this study, the authors propose using massive low-cost passive reflecting elements integrated into a planar surface. [26] presents a comprehensive overview of IRS-aided wireless communications covering channel models, hardware architecture, and practical constraints, as well as various forward looking applications in wireless networks. To facilitate an IRS-based channel estimation, [27] proposes a cooperative beam training scheme. In particular, the authors offer two different hierarchical codebooks for their proposed training procedure to achieve tradeoffs betweenrobustness against noise and searching complexities. A low complexity phase shift search scheme is proposed in [28] to reduce the IRS's computational complexity for THz communication in indoor environments. To minimize the total transmit power at the access point (AP), a joint optimization algorithm is proposed in [29]. The algorithm jointly optimizestransmit beamforming at the AP and reflect beamforming at the IRS under a signal-to-interference-plus-noise (SINR) ratio constraint. The authors of [30] design a method to maximize the sum rate with individual rate constraints, in which the IRS location, IRS phase shift, allocation of THz spectrum, and power control for user equipments (UEs) are jointly optimized. An iterative atom pruning based subspace pursuit (IAP-SP) scheme has also been developed for channel estimation and data rate maximization in [31]. Compared to the classical subspace pursuit (SP) scheme, the proposed IAP-SP algorithm can substantially reduce computational complexity while maintaining high accuracy channel estimation.

While the NLoS problem can be addressed using IRS, the high path loss in sub-THz communications still remains a challenging issue. Based on the analysis in [32], the signal-to-noise-ratio (SNR) of IRS-assisted transmissions is almost the same as for forward-only relay-assisted transmissions without the amplification. To solve the NLoS and path-loss problems simultaneously, we propose a relay-assisted network architecture for THz communications. Under our proposed scheme all transmitters in the network are equipped with massive MIMO antenna arrays where a hybrid precoding is selected to support directional transmissions. Then, a leaky waveguide (LWG) together with a codebook assisted hybrid precoding and combining method is proposed. The proposed method can shorten the beam discovery phase, hence reducing the complexity of the beam discovery algorithm. To realize the proposed method, an empirical data-based THz channel model considering atmospheric attenuation is investigated. As an example, an adaptive FHSS approach is invoked to avoid data transmission at vulnerable frequencies. The contributions of this paper are summarized as follows:

1) We propose a fast LWG-assistedthree dimensional (3D) beam discovery scheme capable of determining the best beam direction in a single round trip, i.e., the transmitter sends a beam discovery signal through LWG and the receiver sends a feedback message. Moreover, considering the characteristics of the THz spectrum, the impact of obstacles is also investigated. Compared with the sector sweeping based beam discovery scheme, e.g., IEEE 802.11ad, our method indicates a significant reduction in the time required to achieve beam discovery.To the best of our knowledge, it's the first paper that investigates 3D beam discovery with LWG.
2) To support the proposed beam discovery method, we adopt a data-based channel model to better evaluateatmospheric attenuation on the sub-THz band. The proposed channel model is based on the empirical data available in a public

database, which is tested by researchers in the field of spectroscopy. Subsequently, the proposed channel model has been used to evaluate the frequency selectivity of atmospheric attenuation on the THz or sub-THz band. Furthermore, since the complexity of the CSI based hybrid precoding method is unacceptable when extremely large-scale antenna arrays are used, we consider a codebook-based hybrid precoding method to reduce the precoding complexity of sub-THz transmitters. Moreover, an optimal combining algorithm is developed to support relay-assisted sub-THz communications.

3) To solve frequency selective attenuation during transmissions, an adaptive FHSS based transmission scheme has been considered for data transmission. Specifically, hopping sequences will be generated based on the dynamically updated channel map. The simulation results indicate that the proposed scheme outperforms the transmission scheme without FHSS.

The rest of the paper is organized as follows: the system model, channel model, LWG-assisted beam discovery scheme, codebook-based hybrid precoding method, optimal combining algorithm, and adaptive FHSS approach are described in Section II. The derivations of performance indexes are given in Section III. Simulations results are presented in Section IV. Conclusions are finally drawn in Section V.

Notation: Throughout this paper, J is the imaginary unit, $\min(\cdot)$ is the smallest value of the given parameters, $[\cdot]_{i,j}$ represents the corresponding element of a vector or matrix, $phase(\cdot)$ is the phase value of the given element, $\Pr$ is the probability operation, $\mathbb{E}(\cdot)$ is the expectation operation, $\|\cdot\|_F$ is the Frobenius norm,and $\det(\cdot)$ is the determinant operation.

II. System Model

A. Network Architecture

Let's consider a network consisting of several relays and obstacles with a small base station (SBS): Θ_{SB}, and a number of UEs: Θ_{UE}. Only Θ_{SB} is connected to the core network, i.e., the relays cannot directly obtain data from the core network. A set of relays is defined as $\Phi_{\mathrm{RE}} = \{\Theta^i_{\mathrm{RE}} | \, i = 1, 2, \ldots, N_{\mathrm{re}}\}$, where Θ^i_{RE} is the ith relay, and N_{re} corresponds to the number of relays contained in the network. A set of obstacles is defined as: $\Phi_{\mathrm{OB}} = \{\Theta^m_{\mathrm{OB}} | \, m = 1, 2, \ldots, N_{\mathrm{ob}}\}$, where Θ^m_{OB} is the mth obstacle, and N_{ob} is the number of obstacles contained in the network. In this paper, the coverage of each obstacle is assumed to be circular with radius r_{ca} (each obstacle will block all transmission paths that fall within this range). The SBS, UE, obstacles, and relays are all located on the plane: $\mathbb{R}_{\mathrm{P}}$, where the length and width of the $\mathbb{R}_{\mathrm{P}}$ are denoted by L_{P} and W_{P}, respectively. The locations of SBS, UE, obstaclesand relays are assumed to be uniformly distributed in $\mathbb{R}_{\mathrm{P}}$. The network architecture is shown in Fig. 1. Similar to [33], [34], the transmitters and receivers are assumed to be located on the same planeso only Azimuthal coordinates are considered in this paper.

We assume that SBS, and relays can operate in sub-6Ghz and sub-THz (from 100 GHz to 200 GHz) bands. The sub-THz band is used by downlink for data transmissionand the

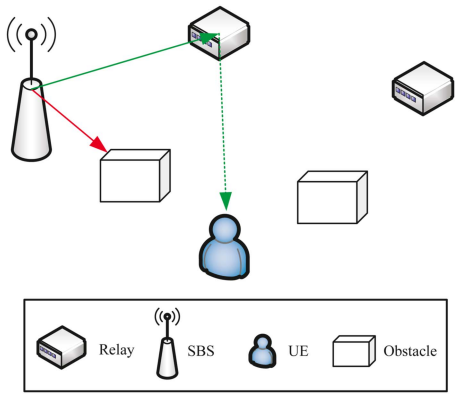

Fig. 1. Network architecture.

sub-6 GHz band is used by uplink to transmit feedback messages. Sincesub-THz is only used in the downlink, we focus mainly ondownlink transmissions. The SBS and relays are equipped with uniform linear antenna arrays (ULA) and omnidirectional antennas. The ULA is used to support massive multiple-input multiple-output (MIMO) technology for data transmissions on the sub-THz band, and the omnidirectional antenna is used to transmit feedback messages on the sub-6 GHz band. Each ULA contains N_{TR} transmitting antennas, while the number of receiving antennas of SBS, UE, and relaysis N_{RC}. The fully connected hybrid precoding architecture is used by the SBS and relays to assist massive MIMO transmissions and the number of radiofrequency (RF) chains is N_{RF}.

The network operates in a time-slotted manner, and the SBS and relays are strictly synchronized. Let ΔT_{L} denote the duration of the time slot. Since ΔT_{L} is small, we can assume that UE: Θ_{UE}, stays static during the ΔT_{L} period. Therefore, there is no need to consider the mobility of Θ_{UE}. Since we consider a time-slot based system, synchronization among devices would require highly accurate time synchronization. For instance, a link-layer synchronization protocol [46] has been proposed for ultra-high-speed wireless communication networks in the THz band. In this approach a receiver initiates a handshake to achieve synchronization between transmitter and receiver in order to maximize the channel utilization. However, to enable highly accurate time synchronization in sub-THz communications, Precision Time Protocol (PTP) [47] is the currently the most advanced protocol and can provide sub-microsecond precision. PTP, which is defined by the IEEE 1588v2 standard [47], uses a handshake mechanism to exchange messages between two nodes through the end-to-end delay measurement. It has been previously applied to 5G time sensitive networks [48] and is considered here to achieve synchronization for beam discovery, as well as the proposed FHSS, which also requires tight synchronization between SBSs, relays and UEs. However, further detail of PTP implantation and its impact on beam discovery and the packet discard probability is well beyond the scope of this paper. Therefore, in this paper we assume that SBSs, relays and UEs are synchronized. Moreover,downlink transmission is divided into two phases; beam discovery and data transmission. Theduration of these two phases are denoted by Δt_{bt} and Δt_{dt},

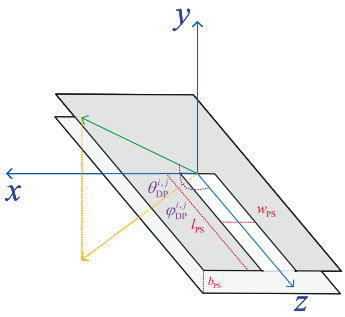

Fig. 2. LWG structure.

respectively. In this paper, we use the leaky waveguide (LWG) to support the beam discovery phase in the sub-THz band.

B. Definition and Configuration of LWG

Although Leaky-Wave devices have been employed in microwave systems for many years, their application in the sub-THz rangehas only recently been investigated [35]. In a typical guided wave implementation, a signal propagating in a waveguide can couple through an aperture to "leak"into free spaceif the guided and free-space modes satisfy a phase-matching condition on their parallel wave vector components. In this paper, we consider the simplest case, i.e., transmitting sub-THz signals witha TE1 transverse electric mode through a metal parallel-plate waveguide with an empty space between plates. In this case, after sub-THz signals pass through the LWG, different frequency components of the sub-THz signal will have different propagating directions due to the phase matching constraint [35]. That is to say, the departing angle of the leaked wave is determined by the frequency of the wave and, if the LWG is excited with a broadband source, each frequency within this broad spectrum should emerge from the slot aperture at one unique angle. The structure of LWG is shown in Fig. 2 [35].

Once a broadband signal passes through the LWG, it will be transformed into a "rainbow"like beam, where different colors indicate different transmission frequencies withunique angles. In this paper, we assume SBS, UE, and relays are equipped with LWG for beam discovery. Since the maximum coverage range of a LWG is 90 degrees on the plane [35], at least four LWGs are needed for each device (if no extra location information of UEs can be achieved by a transmitter).We use the navigation information, e.g., GPS, to achieve a rough estimation of the receivers' locations. A transmitter can then use the information to determine which LWG should be used for beam discovery.Notice that the distance between the transmitter and the receiver is pre-known in [35], and the value of the distance will be used to evaluate the AoA of the discovered LoS path. However, this is not practical in sub-THz band since the transmitting distance of the LoS path is hard to be evaluated due to the attenuations. Thus, in the following section, we will adopt an empirical data based sub-THz channel model to address this issue, and extend the improved LWG-assisted beam discovery method to both SBS and relays.

C. LWG-Assisted Beam Discovery Scheme

Let's define the transmitter as $\mathbf{Ts}_i$, where $i = 0$ represents an SBS, and $i = 1, 2, \ldots, N_{\rm re}$ when the transmitter is a relay. The "rainbow" like beam generated by $\mathbf{Ts}_i$ is further defined as $S^i_{\rm TR}$, where $i = 0$ when the transmitter is an SBS, and $i = 1, 2, \ldots, N_{\rm re}$ when the transmitter is a relay. Similarly, the receiver is defined as $\mathbf{Rc}_j$, where $j = 0$ corresponds to a UE, and $j = 1, 2, \ldots, N_{\rm re}$ if the receiver is a relay. Depending on the receiver's location, only a portion of the sub-THz rainbow can be detected by the receiver, and the received spectrum at the receiver: $\mathbf{Rc}_j$, is denoted as: $S^{i,j}_{\rm RE} \triangleq \{f^{i,j}_{\rm min}, f^{i,j}_{\rm max}, P^{i,j}_{\rm FB}\}$, where $f^{i,j}_{\rm min}$ and $f^{i,j}_{\rm max}$ correspond to the lower and upper bounds of the received spectrum, respectivelyand $P^{i,j}_{\rm FB}$ represents the power of the received signal. As soon as $\mathbf{Rc}_j$ detects $S^{i,j}_{\rm RE}$, a feedback message, $M^{i,j}_{\rm FB} = S^{i,j}_{\rm RE}$, is sent to $\mathbf{Ts}_i$. Under these conditions, the transmitter would be able to know that there is an existing line of sight (LoS) path between the transmitter and receiver.

Thus, for a simple network where there is a LoS path within the Sub-THz transmission range and in the absence of any relay nodes, the beam discovery phase can be carried out using the following steps: 1) Ts_0 generates the sub-THz rainbow $S^0_{\rm TR}$, through LWG, 2) $\mathbf{Rc}_0$ detects $S^{0,0}_{\rm TR}$ and sends a feedback message: $M^{0,0}_{\rm FB}$, to Ts_0, 3) Ts_0 uses the information contained in $M^{0,0}_{\rm FB}$ to initiate the beam discovery. It is important to note that the LWG based method can only be considered when there is a LoS path [35].However, in the case of a network with relay nodes and obstacles (see Fig. 1) the beam discovery process will be carried out with the help of relays. Recall that the SBS and relays are synchronized, sothey can begin the beam discovery phase simultaneously. Moreover, since it is unlikely that different transmission paths from different transmitters have the same transmission direction. Therefore, the probability that the UE receives the same spectrum from different relays or SBSs (if there is more than one SBS) is negligible enough to be ignored. That is to say, we do not need to considerinterference duringa beam training phase. Thus, the beam discovery process can be carried outusing the following steps:

1) At the beginning of each beam discovery phase, the SBS; $\Theta_{\rm SB}$, and relays: $\Theta^k_{\rm RE}$, generate $S^i_{\rm TR}$ independently. Let's define a typical transmitter as $\mathbf{Ts}_i$. Once the receiver: $\mathbf{Rc}_j$, detects $S^{i,j}_{\rm TR}$, a feedback message: $M^{i,j}_{\rm FB}$, will be sent to $\Theta^k_{\rm RE}$ and $\Theta_{\rm SB}$ through the omnidirectional antenna operating on the sub-6 GHz band. If there are no obstacles between the transmitter and the receiver, the transmitter, $\mathbf{Ts}_i$ will receive multiple feedback messages from the receiver as well asnearby relay nodes. In this case, both transmitter and receiver will use the information contained in $M^{i,j}_{\rm FB}$ to estimate AoD, AoA, and channel information. Also, if there is no obstacle between $\Theta_{\rm SB}$ and $\Theta_{\rm UE}$, $\Theta_{\rm SB}$ will receive a feedback message: $M^{0,0}_{\rm FB}$, from $\Theta_{\rm UE}$. In this case, the beam discovery phase will endand the data transmission phase will begin.
2) If the $\Theta_{\rm SB}$ does not receive $M^{0,0}_{\rm FB}$ within a pre-defined period,the beam discovery phase will continue. Let's define a set of feedback messages that is received

by Θ_{SB} as: $M^0_{\mathrm{FB}} \triangleq \{M^{i,j}_{\mathrm{FB}}\}$. By checking each $M^{i,j}_{\mathrm{FB}}$ contained in M^0_{FB}, Θ_{SB} can learn the existence of LoS paths among relays nodes and Θ_{UE}. If the $M^{i,j}_{\mathrm{FB}}$ contained in M^0_{FB} that can form a set like $\mathcal{M}_{\mathrm{FB}} = \{M^{0,i}_{\mathrm{FB}}, M^{i,j}_{\mathrm{FB}}, M^{j,k}_{\mathrm{FB}}, \ldots, M^{m,n}_{\mathrm{FB}}, M^{n,0}_{\mathrm{FB}}\}$, it means that there exists an available relayed link between Θ_{SB} and Θ_{UE} through relays $\{\Theta^i_{\mathrm{RE}}, \Theta^j_{\mathrm{RE}}, \Theta^k_{\mathrm{RE}}, \ldots, \Theta^m_{\mathrm{RE}}, \Theta^n_{\mathrm{RE}}\}$. Once Θ_{SB} finds $\mathcal{M}_{\mathrm{FB}}$, the beam discovery phase will be endedand then the data transmission phase will begin.

3) If Θ_{SB} doesn't find $\mathcal{M}_{\mathrm{FB}}$, it means that there is no available relayed link between Θ_{SB} and Θ_{UE}. The beam discovery phase will then be ended, in which case the data transmission phase cannot be initiated.

Since there may exist multiple available $\mathcal{M}_{\mathrm{FB}}$s, the one with the smallest number of elements will be the selected in order to minimizetransmission delay. If multiple $\mathcal{M}_{\mathrm{FB}}$s, still exist,the one with the maximum received power, i.e., $P^{i,j}_{\mathrm{FB}}$, will be selected. Notice that all steps can be done within a single round trip, i.e., a transmitter, $\mathbf{Ts}_i$, only needs to generate S^i_{TR} once, and the receiver: $\mathbf{Rc}_j$, only needs to transmit a feedback message: $M^{i,j}_{\mathrm{FB}}$, to $\mathbf{Ts}_i$ and $\mathbf{Ts}_0$ once. Thus, this method is much more efficient than the sector sweeping based beam discovery method, e.g., IEEE 802.11ad. Since we don't consider UEs' mobility, $\mathbf{Rc}_j$ only needs to transmit a feedback message to $\mathbf{Ts}_i$ once the attenuated frequency range changes due toslowly varying weather conditions. Also, the availability of the corresponding received spectrum will be contained in the feedback messages. $\mathbf{Ts}_i$ canthen use this information to improve the performance of the following data transmission phase (more details will be presented in Section II-H). In the followingfor the sake of simplicity in our analysis, we assume a single hop transmission (i.e., only a single relay node is used in each transmission link).

In this section we willevaluate how Θ_{SB} and Θ^i_{RE} use the information contained in $\mathcal{M}_{\mathrm{FB}}$ to perform a hybrid precoding. For a pair of transmitters, $\mathbf{Ts}_i$, and receiver, $\mathbf{Rc}_j$,we can define the azimuth AoD at the transmitter as $\theta^{i,j}_{\mathrm{DP}}$, the azimuth AoA at the receiver as $\theta^{i,j}_{\mathrm{AR}}$, and the distance between $\mathbf{Ts}_i$ and $\mathbf{Rc}_j$ as $R_{i,j}$.Let us assume that $\theta^{i,j}_{\mathrm{DP}} \in [0, \frac{\pi}{2}]$.Defining $f^{i,j}_{\mathrm{FB}} = \{f^{i,j}_{\theta}, f^{i,j}_{\varphi}\}$, based on the phase matching constraintthe relationship of $f^{i,j}_{\theta}$ and azimuth AoD can be expressed by,

$$f^{i,j}_{\theta} = \frac{C_{\mathrm{LI}}}{2b_{\mathrm{PS}} \sin\left(\theta^{i,j}_{\mathrm{DP}}\right)}, \tag{1a}$$

where C_{LI} is the velocity of light ina vaccum, and b_{PS} is the plate separation of the LWG. Notice that in [35] the distance between $\mathbf{Ts}_i$ and $\mathbf{Rc}_j$ is configured to be a fixed value. Thus, in this paper, the transmission distance $R_{i,j}$ needs to be estimatedfirst.Then, based on [35], the value of azimuth AoA, i.e., $\theta^{i,j}_{\mathrm{AR}}$ can be achieved once the transmission distance $R_{i,j}$ is estimated.

Based on [36], the LWG shown in Fig. 2 cannot be used for 3D beam discovery. Because we need to increase the width of the slot, w_{PS}, to make a wider beam on the x-z (i.e., elevation) plane to realize 3D beam discovery. However, this solution is practical at lower frequencies, e.g., sub-6 GHz, but not practical when higher frequencies are used. When the slot width increases, the sides of the slot act as secondary leaking structures, and the frequency-angle relationship in (1a) is not obeyed as the energy at a given frequency is radiated in a broad range of angles. Thus, to realize LWG-assisted 3D beam discovery, the structure of the LWG needs to be changed. To address this problem, we use an alternate slot aperture, in which the slot width increases linearly along its length (i.e., a trapezoidal shape) [37]. By doing experiments, the authors of [37] find that with a trapezoidal-shaped slot, the two sides of the slot as a pair of secondary leaking structures follow their own phase-matching condition in the x-z plane without influencing the phase-matching condition in the y-z (i.e., azimuth) plane.

Then, the relationship of $f^{i,j}_{\varphi}$ and elevation AoD, $\varphi^{i,j}_{\mathrm{DP}}$, can be expressed by,

$$f^{i,j}_{\varphi} = \frac{C_{\mathrm{LI}}}{2b_{\mathrm{PS}} \sin\left(\varphi^{i,j}_{\mathrm{DP}}\right)}. \tag{1b}$$

Similarly, the value of elevation AoA, i.e., $\varphi^{i,j}_{\mathrm{AR}}$ can be achieved once the transmission distance $R_{i,j}$ is estimated.

D. Pathloss With Atmospheric Attenuation

To estimate the value of $R_{i,j}$, we need to investigate the relationship between $P^{i,j}_{\mathrm{FB}}$ and $R_{i,j}$. Moreover, since transmission onthe sub-THz spectrum is frequency selective, the value of $P^{i,j}_{\mathrm{FB}}$ is related to the received spectrum. Fortunately, there is no need to consider the multi-path effect sinceLWG is used. Based on [38], [40], [41], signal loss on the transmission path can be expressed as:

$$\begin{aligned}\alpha_{\mathrm{PL}}\left(f_{\mathrm{TS}}, \mathcal{R}\right) &= \mathcal{L}_{\mathrm{SP}}\left(f_{\mathrm{TS}}, \mathcal{R}\right) \mathcal{L}_{\mathrm{ABS}}\left(f_{\mathrm{TS}}, \mathcal{R}\right) \\ &= \left(\frac{C_{\mathrm{LI}}}{4\pi f_{\mathrm{TS}} \mathcal{R}}\right)^2 e^{-k_{\mathrm{abs}}(f_{\mathrm{TS}})\mathcal{R}}, \end{aligned} \tag{2}$$

where f_{TS} is the frequency of the signal, $\mathcal{L}_{\mathrm{SP}}(f_{\mathrm{TS}}, \mathcal{R})$ is the spreading loss, $\mathcal{L}_{\mathrm{ABS}}(f_{\mathrm{TS}}, \mathcal{R})$ is the molecular absorption loss, and $k_{\mathrm{abs}}(f_{\mathrm{TS}})$ is the frequency-dependent medium absorption coefficient, which is determined by the composition of the transmission medium at a molecular level. Based on [40], $k_{\mathrm{abs}}(f_{\mathrm{TS}})$ can be expressed as:

$$k_{\mathrm{abs}}\left(f_{\mathrm{TS}}\right) = \sum_{h,g} k_{h,g}\left(f_{\mathrm{TS}}\right) \tag{3}$$

$k_{h,g}(f_{\mathrm{TS}})$ stands for the individual absorption coefficient for the isotopologue h of gas g. For example, the air in an office is mainly composed of nitrogen (78.1%), oxygen (20.9%) and water vapor (0.1–10.0%). Each gas has different resonatingisotopologues within the THz or sub-THz band, i.e., molecules that only differ in their isotopic composition. $k_{h,g}(f_{\mathrm{TS}})$ can be further expressed as:

$$k_{h,g}\left(f_{\mathrm{TS}}\right) = \frac{\mathcal{P}}{\mathcal{P}_0} \frac{\mathcal{T}_{\mathrm{STP}}}{\mathcal{T}} Q_{h,g} \sigma_{h,g}\left(f_{\mathrm{TS}}\right), \tag{4}$$

where $\mathcal{P}$ is the pressure and $\mathcal{T}$ is the temperature of the environment, $\mathcal{P}_0$ and $\mathcal{T}_{\mathrm{STP}}$ are the Standard-Pressure-Temperature values, $Q_{h,g}$ is the total number of molecules per volume unit, and

$\sigma_{h,g}(f_{\mathrm{TS}})$ is the absorption cross-section for the isotopologue h of gas g in $\mathrm{m}^2/\mathrm{molecule}$. Simply stated, the total absorption depends on the number of molecules of a given gasfound along the path. Based on [40], $Q_{h,g}$ can be further derived by:

$$Q_{h,g} = \frac{\mathcal{P}}{\mathcal{R}_{\mathrm{C}}\mathcal{T}} q_{h,g} N_{\mathrm{A}}, \tag{5}$$

where $q_{h,g}$ is the mixing ratio for the isotopologue h of gas g, N_{A} stands for the Avogadro constant, and $\mathcal{R}_{\mathrm{C}}$ is the gas constant. Based on the discussions in [38], ina high-resolution transmission molecular absorption database (HITRAN), the contribution of each isotopologueis scaled according to its natural abundance in the medium. Therefore, the mixing ratio of the specific gas, q_g, should be used for allisotopologues of g, instead ofindividual mixing ratios $q_{h,g}$. Furthermore, $\sigma_{h,g}(f_{\mathrm{TS}})$ in (4) can be shown as:

$$\sigma_{h,g}\left(f_{\mathrm{TS}}\right) = S_{h,g} G_{h,g}\left(f_{\mathrm{TS}}\right), \tag{6}$$

where $S_{h,g}$ is the line intensity for the absorption of the isotopologue h of gas g, and $G_{h,g}(f_{\mathrm{TS}})$ is the spectral line shape, which can be expressed by:

$$G_{h,g}\left(f_{\mathrm{TS}}\right) = \frac{f_{\mathrm{TS}}}{f_{h,g}^{\mathrm{C}}} \frac{\tanh\left(\frac{H_{\mathrm{PL}} C_{\mathrm{LI}} f_{\mathrm{TS}}}{2 k_B \mathcal{T}}\right)}{\tanh\left(\frac{H_{\mathrm{PL}} C_{\mathrm{LI}} f_{h,g}^{\mathrm{C}}}{2 k_B \mathcal{T}}\right)} F_{h,g}\left(f_{\mathrm{TS}}\right), \tag{7}$$

where H_{PL} is the Planck constant, and k_B stands for the Boltzmann constant. $f_{h,g}^{\mathrm{C}}$ is the position of the resonant frequency that can be expressed as,

$$f_{h,g}^{\mathrm{C}} = f_{h,g}^{\mathrm{C0}} + \delta_{h,g} \frac{\mathcal{P}}{\mathcal{P}_0}, \tag{8}$$

where $f_{h,g}^{\mathrm{C0}}$ is the zero-pressure position of the resonance, and $\delta_{h,g}$ is the linear pressure shift. $F_{h,g}(f_{\mathrm{TS}})$ in (7) is the Van Vleck-Weisskopf asymmetric line shape [42], which is used to represent the molecular absorption.

$$\begin{aligned} F_{h,g}\left(f_{\mathrm{TS}}\right) = {} & 100 C_{\mathrm{LI}} \frac{\alpha_{h,g}^{\mathrm{LO}}}{\pi} \frac{f_{\mathrm{TS}}}{f_{h,g}^{\mathrm{C}}} \cdot \\ & \left(\frac{1}{\left(f_{\mathrm{TS}} - f_{h,g}^{\mathrm{C}}\right)^2 + \left(\alpha_{h,g}^{\mathrm{LO}}\right)^2} + \frac{1}{\left(f_{\mathrm{TS}} + f_{h,g}^{\mathrm{C}}\right)^2 + \left(\alpha_{h,g}^{\mathrm{LO}}\right)^2} \right), \end{aligned} \tag{9}$$

with the Lorentz half-width $\alpha_{h,g}^{\mathrm{LO}}$ as:

$$\begin{aligned} \alpha_{h,g}^{\mathrm{LO}} = {} & \left(\left(1 - q_{h,g}\right) \alpha_0^{\mathrm{air}} + q_{h,g} \alpha_0^{h,g} \right) \cdot \\ & \left(\frac{\mathcal{P}}{\mathcal{P}_0} \right) \left(\frac{\mathcal{T}_0}{\mathcal{T}} \right)^{\gamma_{\mathcal{T}}}, \end{aligned} \tag{10}$$

where $\mathcal{T}_0$ is the reference temperature, $\gamma_{\mathcal{T}}$ is the temperature broadening coefficient, α_0^{air} is the air half-widths, and $\alpha_0^{h,g}$ is the self-broadened half-widths.

All the aforementioned parameters can be directly obtained from the HITRAN database. As we know, the absorption coefficient is highly frequency-selective. This feature will also be reflected in the path loss, e.g., (2). The simulation results of (2) are shown in Fig. 2.

Due to the atmospheric attenuation, we can see that the value of the path loss coefficient is highly related to the frequency of the signal. Notice that not only water vapor, but also nitrogen and oxygen can cause the frequency selective attenuation. Moreover, parameter q_g also has a strong impact on path loss. In Fig. 2 we compare the path loss value with four different moisture contents by changing q_g, where g represents $\mathrm{H_2O}$.

E. Transmission Range of LWG

Based on the discussion in Sections II-B, C and D, the AoD and the AoA of the discovered LoS path can be derived based on the feedback information. Hence, the transmission range of LWGs needs to be large enough to ensure the receivers can detect the transmitted signal. However, when the transmission power is at the microwatt-level, the LWGhas only a centimeter-level coverage range [35]. To solve this problem, we can narrow the radiation range of LWGs, i.e., making the LWG beams more directional.Take the transmission in the azimuth plane as an example, by reducing the frequency range of the broadband sources used by Ts_i, the transmit power of each frequency component contained in S_{TR}^i can be enhanced without increasing the generating power of the broadband sources. However, based on the phase-matching constraint, a smaller frequency range of the broadband source leads to a narrower LWG beam coverage. For example, based on [35], if we reduce the maximum frequency of the broadband source from 2 THz to 146 GHz, based on (1) the coverage of LWG will be narrowed to 10 degrees instead of 90 degrees. On the other hand, to realize a meter-level transmission range of LWG, the following inequality needs to be satisfied

$$P_{\mathrm{req}} Eh\left(\varphi_{\mathrm{req}}\right) \alpha_{\mathrm{PL}}\left(f_{\mathrm{ref}}, d_{\mathrm{req}}\right) \geq P_{\mathrm{ref}} \alpha_{\mathrm{PL}}\left(f_{\mathrm{ref}}, d_{\mathrm{ref}}\right), \tag{11a}$$

where P_{req} is the required transmit power, $\alpha_{\mathrm{PL}}(f_{\mathrm{ref}}, d_{\mathrm{req}})$ is the path loss with reference frequency $f_{\mathrm{ref}} = 100\,\mathrm{GHz}$, and the required transmit distance between the transmitter $\mathbf{Ts}_i$ and receiver $\mathbf{Rc}_j$ is $R_{i,j}$, $P_{\mathrm{ref}} = 10\,\mu\mathrm{W}$ is the transmit power in [35], and $\alpha_{\mathrm{PL}}(f_{\mathrm{ref}}, d_{\mathrm{ref}})$ is the path loss with reference frequency $f_{\mathrm{ref}} = 100\,\mathrm{GHz}$ and $d_{\mathrm{req}} = 0.1\,\mathrm{m}$. $Eh(\varphi_{\mathrm{req}})$ is the beam width (i.e., φ_{req}) related enhancement on the received power, which is expressed by

$$Eh\left(\varphi_{\mathrm{req}}\right) = \frac{\left(f_{\max}^{\mathrm{ref}} - f_{\mathrm{cut}}\right)}{\left(\frac{f_{\mathrm{cut}}}{\sin(\pi(1/2 - \varphi_{\mathrm{req}}/180))} - f_{\mathrm{cut}}\right)}, \tag{11b}$$

where $f_{\mathrm{cut}} = C_{\mathrm{LI}}/2b_{\mathrm{PS}}$ is the cutoff frequency of the LWG, and $f_{\max}^{\mathrm{ref}} = 2\,\mathrm{THz}$ is the maximum frequency of the broadband source used in [35].

By solving (11a), the relation between the required transmit power and the LWG beam width is shown in Fig. 3.

Based on Fig. 3, the required transmit power P_{req} increases with the LWG beamwidth. Specifically, compared with [35], when $\varphi_{\mathrm{req}} \leq 3$, the required transmit power P_{req} is less than $P_{\mathrm{ref}} = 10\,\mu\mathrm{W}$. This observation indicates that we don't need to increase the transmit power of LWG sources in the beam discovery phase if we set the beam widthto less than 30 degrees when $R_{i,j} = 10\,\mu\mathrm{m}$. Moreover, if we can increase the transmit power to1 mW when $R_{i,j} = 10\,\mu\mathrm{m}$, a beam width of 30 degrees can be used for beam discovery. Here we set the beamwidth of LWG as $\varphi_{\mathrm{req}} = 30$ degrees. Since the navigation information, e.g., GPS, is used to provide rough location estimations of the

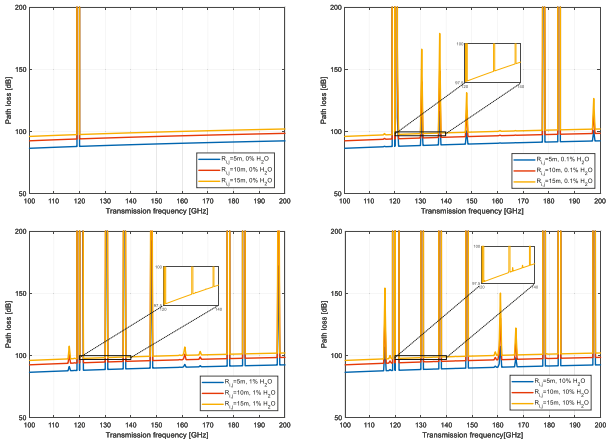

Fig. 3. Path loss coefficient versus signal frequency and moisture content.

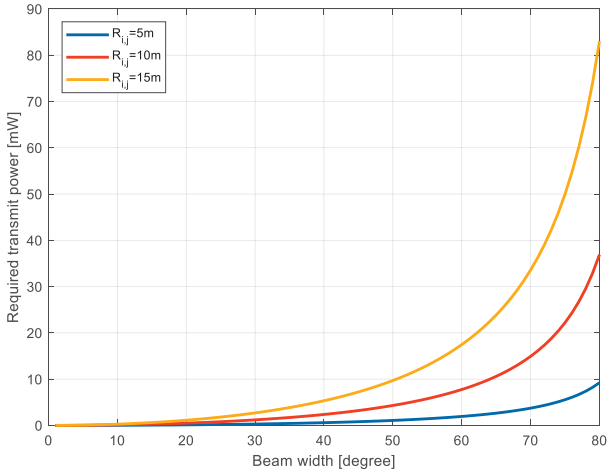

Fig. 4. Required transmit power versus LWG beam width with respect to $R_{i,j}$.

receivers, the smaller LWG beamwidth will not influence the efficiency of the proposed beam discovery method.

F. Codebook-Based Hybrid Precoding

As we can see from Fig. 3, the value of the path loss coefficient largely depends on the frequency of the signal. The relationship between the power of the received signal $P_{\mathrm{FB}}^{i,j}$ and transmission power P_{TR} is,

$$P_{\mathrm{FB}}^{i,j} = P_{\mathrm{TR}} \left(\frac{C_{\mathrm{LI}}}{4\pi f_{\mathrm{C}}^{i,j} R_{i,j}} \right)^2 e^{-k_{\mathrm{abs}}(f_{\mathrm{C}}^{i,j}) R_{i,j}}, \tag{12}$$

where $f_{\mathrm{C}}^{i,j}$ is the received spectrum of $\mathbf{Rc}_j$, which is included in the feedback message. Since the values of $P_{\mathrm{FB}}^{i,j}$, P_{TR} and $f_{\mathrm{C}}^{i,j}$ are already known, we can use (12) to evaluate the transmission distance $R_{i,j}$. Based on [35], the LWG receiver can detect signals at the μW level, which is much lower than the signal power used to transmit data. Therefore, if the receiver can detect the beam discovery signal, then the power used for transmitting data is large enough for the receiver to detect. Without a loss of generality, we can assume that the transmit power for both data and beam discovery (after passing LWG) is the same. Now, we can obtain the value of $\theta_{\mathrm{DP}}^{i,j}$, $\alpha_{\mathrm{PL}}(f_{\mathrm{C}}^{i,j}, R_{i,j})$, and $\theta_{\mathrm{AR}}^{i,j}$, based on [35]. The channel matrix between transmitter and receiver can be shown as (13).

$$\mathbf{H} = \begin{bmatrix} h_{1,1} & h_{1,2} & \cdots & h_{1,N_{\mathrm{TR}}} \\ h_{2,1} & h_{2,2} & \cdots & h_{2,N_{\mathrm{TR}}} \\ \vdots & \vdots & \vdots & \vdots \\ h_{N_{\mathrm{RC}},1} & h_{N_{\mathrm{RC}},2} & \cdots & h_{N_{\mathrm{RC}},N_{\mathrm{TR}}} \end{bmatrix}_{N_{\mathrm{RC}} \times N_{\mathrm{TR}}}, \tag{13}$$

where $h_{Ar,At}$ is the channel gain between the transmitting antenna, At, and the receiving antenna, Ar. N_{TR} and N_{RC} are the number of transmitting and receiving antennas, respectively. Based on [38], $\mathbf{H}$ can be obtained as,

$$\mathbf{H} = \alpha_{\mathrm{PL}} \left(f_{\mathrm{C}}^{i,j}, R_{i,j} \right) G_{\mathrm{TR}} G_{\mathrm{AR}} \times \mathbf{a}_{\mathrm{TR}} \left(\varphi_{\mathrm{DP}}^{i,j}, \theta_{\mathrm{DP}}^{i,j} \right) \mathbf{a}_{\mathrm{AR}} \left(\varphi_{\mathrm{AR}}^{i,j}, \theta_{\mathrm{AR}}^{i,j} \right)^H. \tag{14}$$

where G_{TR} and G_{AR} are the transmit and receive antenna gains, vectors $\mathbf{a}_{\mathrm{TR}}(\varphi_{\mathrm{DP}}^{i,j}, \theta_{\mathrm{DP}}^{i,j})$ and $\mathbf{a}_{\mathrm{AR}}(\varphi_{\mathrm{DP}}^{i,j}, \theta_{\mathrm{DP}}^{i,j})$ represent the array steering vectors at the transmitter and receiver sides, respectively.For a $M_x \times M_y$ elements uniform plane array (UPA), the array steering vector can be expressed by (15),

$$\mathbf{a}_{\mathrm{UPA}}(\varphi, \theta) = \Big[1, \ldots, e^{J\pi(m_x \sin\varphi \sin\theta + m_y \cos\theta)}, \ldots, e^{J\pi((M_x-1)\sin\varphi\sin\theta + (M_y-1)\cos\theta)} \Big]^T. \tag{15}$$

where m_x and m_y are the antenna element index with $0 \le m_x \le Mx$ and $0 \le m_y \le My$, respectively; r_{A} is the antenna element spacing, J is the imaginary unit, and λ_{C} is the wavelength.

Now channel matrix $\mathbf{H}$ can be estimated with the help of LWG. As soon as $\mathbf{H}$ is estimated, the beam discovery phase will end. Based on the estimated $\mathbf{H}$, the transmitter needs to determine the beam pattern for the data transmission phase. Here we use a codebook based hybrid beamforming method [39]. The constructed codebook $\mathbf{CB}_{\mathrm{S}}$ is shown in Fig. 4.

Here $\{\mathbf{F}_{\mathrm{CB}}^i = \mathbf{F}_{\mathrm{RF}}^i \mathbf{F}_{\mathrm{BB}}^i | \ i \in [1, \mathrm{NRs}]\}$ is the codeword of the codebook $\mathbf{CB}_{\mathrm{S}}$, where $\mathbf{F}_{\mathrm{RF}}^i$ is the i th codeword of the RF precoder, $\mathbf{F}_{\mathrm{BB}}^i$ is the i th codeword of the baseband precoder, and NRs is the number of beam patterns contained in $\mathbf{CB}_{\mathrm{S}}$. The construction process of the codebook can be done with the algorithm used in [43].

The transmitter can then determine the beam pattern $\mathbf{F}_{\mathrm{CB}}^*$ from $\mathbf{CB}_{\mathrm{S}}$ by,

$$\mathbf{F}_{\mathrm{CB}}^* = \underset{\mathbf{F}_{\mathrm{CB}}^i \in \mathbf{CB}_{\mathrm{S}}}{\arg\max} \det \left(\mathbf{I}_{N_{\mathrm{RC}}} + \frac{P_{\mathrm{TR}}}{\sigma_s^2} \mathbf{H} \mathbf{F}_{\mathrm{CB}}^i (\mathbf{F}_{\mathrm{CB}}^i)^H \mathbf{H}^H \right), \tag{16}$$

where $\det(\cdot)$ is the determinant of a given matrix and the spectral efficiency can be expressed by,

$$C_{\mathrm{AD}} = \log_2 \det \left(\mathbf{I}_{N_{\mathrm{RC}}} + \frac{P_{\mathrm{TR}}}{\sigma_{\mathrm{s}}^2} \mathbf{H} \mathbf{F}_{\mathrm{CB}}^* (\mathbf{F}_{\mathrm{CB}}^*)^H \mathbf{H}^H \right), \tag{17}$$

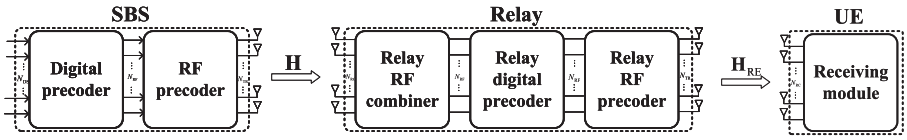

Fig. 5. Transmission between a SBS and a UE through a relayed path.

where σ_s^2 is the power of additive white Gaussian noise (AWGN) of the channel between the SBS and UE and $\mathbf{I}_{N_{\mathrm{RC}}}$ is an $N_{\mathrm{RC}} \times N_{\mathrm{RC}}$ identity matrix. However, based on (16), we need to compute the determinant of a given matrix before we find the codeword. This operation has a $O(N_{\mathrm{TR}}^3)$ temporal complexity. Furthermore, this action will repeat NRs times to find the maximum value among the NRs candidates.It is practical when $\mathrm{N_{TR}}$ and NRs are small, but not acceptable in our case.

Based on [44], the channel matrix can be singular decomposed and further expressed as,

$$\mathbf{H} = \mathbf{U}\boldsymbol{\Sigma}\mathbf{V}^H = \sum_{k=1}^{L_{\mathrm{PP}}} A_k \mathbf{u}_k \mathbf{v}_k^H \ , \tag{18}$$

where $\mathbf{u}_k$ and $\mathbf{v}_k$ are the kth vectors in matrices $\mathbf{U}$ and $\mathbf{V}$, respectively. The singular values, A_k, are assumed to be in a descending order. L_{PP} is the rank of the channel andequal to the number of propagation paths for the transmission scenario. Note that for sub-THz systems, the channels usually have limited scattering characteristics, which means the number of propagation paths is far less than $\min(N_{\mathrm{TR}},\ N_{\mathrm{RC}})$. In such cases, the channel rank is equal to the number of propagation paths L_{PP}. Moreover, since we are only considering transmissions with LoS paths, (18) can be further simplified as $\mathbf{H} = \mathcal{A}_s \mathbf{u}\mathbf{v}^H$. The optimal codeword $\mathbf{F}_{\mathrm{CB}}^*$, which maximizes the spectral efficiency, C_{AD}, will satisfy the following condition:

$$\begin{aligned} &phase\left([\mathbf{F}_{\mathrm{CB}}^*]_{:,m}\right) = phase\left([\mathbf{v}]_m\right) \ , \\ &\forall m = 1, 2, ..., N_{\mathrm{TR}}, \end{aligned} \tag{19}$$

where $[\cdot]_{i,j}$ represents the corresponding element of a vector or matrix, $[\cdot]_{:,m}$ means an arbitrary element in the m th column of the corresponding matrix, and $phase(\cdot)$ is the phase value of the element. Comparing equation $\mathbf{H} = \mathcal{A}_s \mathbf{u}\mathbf{v}^H$ with (14), we can easily notice that $\mathbf{v} = \mathbf{a}_{\mathrm{TR}}(\theta_{\mathrm{DP}}^{i,j})$. Thus, the optimal codeword, $\mathbf{F}_{\mathrm{CB}}^*$ depends only on the value of $\theta_{\mathrm{DP}}^{i,j}$, i. e., the transmitters can directly use the codeword that corresponds to $\theta_{\mathrm{DP}}^{i,j}$, instead of requiring complex optimizations. This method also has another advantage in that the value of $\theta_{\mathrm{DP}}^{i,j}$ can also be obtained at the receiver $\mathbf{Rc}_j$. In other words, $\mathbf{F}_{\mathrm{CB}}^*$ can be obtained at both receiver, $\mathbf{Rc}_j$, and transmitter, $\mathbf{Ts}_i$. In addition, $\mathbf{Rc}_j$ can further use $\mathbf{F}_{\mathrm{CB}}^*$ to perform an optimal combining.

G. Optimal Combining at Relay Side

If there is no LoS path between SBS and UE, then relays should be used to support the communication. In this paper, the relay is not connected to the core network for the sake of reducing installation cost. Also, data transmitted to relays only needs to be decomposed instead of decoded in order to reduce the complexity.

Algorithm 1: Construction of Combining Matrix.

$\mathbf{W}_{\mathrm{RF}} = \text{Empty Matrix};$
$\mathbf{W}_{\mathrm{res}} = \mathbf{W}_{\mathrm{MMSE}};$
for $i \leq N_{\mathrm{RF}}$ **do**
  $\mathbf{T} = \boldsymbol{\alpha}_{\mathrm{AR}}(\theta_{\mathrm{AR}}^{i,j})\mathbb{E}(\mathbf{y}\mathbf{y}^H)\mathbf{W}_{\mathrm{res}};$
  $k = \mathbf{T}\mathbf{T}^H;$
  $\mathbf{W}_{\mathrm{RF}} = [\mathbf{W}_{\mathrm{RF}} | [\mathbf{A}_{\mathrm{can}}]_{:,k}];$
  $\mathbf{W}_{\mathrm{DG}} = (\mathbf{W}_{\mathrm{RF}}^H \mathbb{E}(\mathbf{y}\mathbf{y}^H)\mathbf{W}_{\mathrm{RF}})^{-1} \times \mathbf{W}_{\mathrm{RF}}^H \mathbb{E}(\mathbf{y}\mathbf{y}^H)\mathbf{W}_{\mathrm{MMSE}};$
  $\mathbf{W}_{\mathrm{res}} = \frac{\mathbf{W}_{\mathrm{MMSE}} - \mathbf{W}_{\mathrm{RF}}\mathbf{W}_{\mathrm{DG}}}{\|\mathbf{W}_{\mathrm{MMSE}} - \mathbf{W}_{\mathrm{RF}}\mathbf{W}_{\mathrm{DG}}\|_F};$
end for
$\mathbf{W}_{\mathrm{RE}} = \frac{\mathbf{W}_{\mathrm{RF}}\mathbf{W}_{\mathrm{DG}}}{\|\mathbf{W}_{\mathrm{RF}}\mathbf{W}_{\mathrm{DG}}\|_F}$

In the rest of the paperwe only consider a single relay in order to simplify the derivations. As shown in Fig. 5, the transmitted signal from the SBS will be combined at the relay and then transmitted to the user after hybrid precoding. Since we are mainly focused on the beam discovery process for SBSs and relay nodes, the combining process at an UEs has not been considered. Under these conditions, the spectral efficiency of transmission from the SBS to the UE through only a single relay can be expressed as (20).

$$\begin{aligned} C_{\mathrm{AR}} = \log_2 \det \Bigg(&\mathbf{I}_{N_{\mathrm{DS}}} + \frac{P_{\mathrm{TR}}}{N_{\mathrm{DS}}} \mathbf{H}_{\mathrm{RE}} \mathbf{F}_{\mathrm{RB}}^* \mathbf{R}_{\mathrm{n}}^{-1} \mathbf{W}_{\mathrm{RE}}^H \mathbf{H} \\ &\times \mathbf{F}_{\mathrm{CB}}^* (\mathbf{F}_{\mathrm{CB}}^*)^H \mathbf{H}^H \mathbf{W}_{\mathrm{RE}} (\mathbf{F}_{\mathrm{RB}}^*)^H \mathbf{H}_{\mathrm{RE}}^H \Bigg), \end{aligned} \tag{20}$$

where $\mathbf{H}_{\mathrm{RE}}$ is the channel matrix for transmission between a relay and a UE. $\mathbf{W}_{\mathrm{RE}}$ is the combining vector at the relay side, $\mathbf{F}_{\mathrm{RB}}^*$ is the codeword that is selected by the relay, and N_{DS} is number of data streams at the transmitter side. $\mathbf{R}_{\mathrm{n}} = \sigma_s^2 \mathbf{W}_{\mathrm{RE}}^H \mathbf{W}_{\mathrm{RE}}$ is the noise covariance matrix after the combining process.

Notice that codebook $\mathbf{CB}_{\mathrm{R}}$ is constructed to supporthybrid precoding. However, the combining matrix $\mathbf{W}_{\mathrm{RE}}$ is yet to be determined. Withhelp of the method proposed in [45], the following Algorithm 1 can be used at the relay node to obtainoptimal $\mathbf{W}_{\mathrm{RE}}$ when codeword $\mathbf{F}_{\mathrm{CB}}^*$ is determined.

The received signal, $\mathbf{y}$, can be expressed as,

$$\mathbf{y} = P_{\mathrm{TR}} \mathbf{H} \mathbf{F}_{\mathrm{CB}}^* \mathbf{s} + \mathbf{n} \ , \tag{21}$$

$\mathbf{s}$ is the transmitted data stream, and $\mathbf{n}$ is the vector of i.i.d. AWGN. Thus, $\mathbb{E}(\mathbf{y}\mathbf{y}^H)$ can be shown as,

$$\mathbb{E}\left(\mathbf{y}\mathbf{y}^H\right) = \frac{P_{\mathrm{TR}}}{N_{\mathrm{DS}}} \mathbf{H} \mathbf{F}_{\mathrm{CB}}^* (\mathbf{F}_{\mathrm{CB}}^*)^H \mathbf{H}^H + \sigma_s^2 \mathbf{I}_{N_{\mathrm{TR}}} \ , \tag{22}$$

where N_{DS} is the number of data streams contained in $\mathbf{s}$. Notice that a relay node only requires $\mathbb{E}(\mathbf{y}\mathbf{y}^H)$ to execute Algorithm 1, as it already has the information of channel matrix, $\mathbf{H}$, and codeword, $\mathbf{F}^*_{\mathrm{CB}}$. Thus, the exact value of $\mathbf{y}$, which needs to be decoded at the relay, is not necessary for combining. $\mathbf{W}_{\mathrm{MMSE}}$ in Algorithm-1 is expressed by (23).

$$\mathbf{W}_{\mathrm{MMSE}} = \left(\frac{1}{P_{\mathrm{TR}}} \left((\mathbf{F}^*_{\mathrm{CB}})^H \mathbf{H}^H \mathbf{H} \mathbf{F}^*_{\mathrm{CB}} + \frac{\sigma^2 N_{\mathrm{DS}}}{P^2_{\mathrm{TR}}} \mathbf{I}_{N_{\mathrm{DS}}} \right)^{-1} \times (\mathbf{F}^*_{\mathrm{CB}})^H \mathbf{H}^H \right)^H \tag{23}$$

And $\mathbf{A}_{\mathrm{can}}$ is expressed by (24),

$$\mathbf{A}_{\mathrm{can}} = \left[\boldsymbol{\alpha}_{\mathrm{UPA}}(0), \boldsymbol{\alpha}_{\mathrm{UPA}} \left(\frac{\pi}{\mathrm{NRs}} \right), \ldots, \boldsymbol{\alpha}_{\mathrm{UPA}} \left(\frac{(N_{\mathrm{ca}} - 2)\,\pi}{\mathrm{NRs}} \right), \boldsymbol{\alpha}_{\mathrm{UPA}} \left(\frac{(N_{\mathrm{ca}} - 1)\,\pi}{\mathrm{NRs}} \right) \right], \tag{24}$$

where N_{ca} is a constant. As an example, we set $N_{\mathrm{ca}} = 512$ in this paper.

H. Adaptive FHSS Approach

As mentioned in Section II-D, there are severe atmospheric attenuations at certain frequency ranges due to molecular absorption (See Fig. 9). Bear in mind that such attenuations are a function of frequency and molecular absorption lossesand can fluctuate from time-to-time depending on the local atmospheric conditions. Under these conditions, selection of an appropriate carrier frequency can be considered to mitigate such attenuations.This would require feedback from the LWG receiver where the attenuated regions, at certain frequencies, can be identified at the LWG receiver (as shown in Fig. 9). At the receiver, the identified frequency range of the attenuated regions within the broadband spectrum of the sub-THz can then be transmitted to the base station. This information will be in addition to the channel feedback information, such as AoA and AoD. Upon receiving the feedback, the base station can takethe appropriate action to avoid transmission at these frequencies. Since humidity and temperature, especially at a fixed users location, are expected to change very slowly, the channel condition only needs to be updated from time to time. In the other words, the range of attenuated frequencies, within the allocated spectrum, can be included in the feedback whenever it is needed. We should point out, however, that under high speed mobility conditions, the atmospheric channel conditions can lead to faster channel variation, in which case the vulnerable frequencies within the allocated spectrum need to be updated more frequently.

The channeling effect can be compensated by shifting the transmission frequency or changing modulations and coding to prevent or reduce the impact of any partial overlaps within an attenuated region. For example, in this paper we consider Frequency Hopping Spread Spectrum (FHSS) where the carrier frequency of the transmit signal hops among multiple discrete carrier frequencies based on a unique spreading sequence. The main idea is to avoid using hopping frequencies within the attenuate regions. In addition, FHSS has the advantage of being resistant to jamming due to its unique frequency-hopping pattern.

In our adaptive FHSS approach, a channel map is maintained and updated by all equipment once the frequency range of the attenuated regions is identified by the LWG receiver and subsequently transmitted to the base station. Please note that all UEs will attain the same channel map since they are in a small area due to the short range of sub-THz communication and hence, havethe same local atmospheric conditions. Channels will be categorized as usable or un-usable according to the dynamically updated channel map. A set of orthogonal hopping sequences will be generated by using the same frequency hopping sequence generator where every UE will be assigned a specific hopping sequence. For example, the ith UE will be assigned the jth hopping sequence. This order is distributed to UEs from the base station in the association process. In this way, UEs can correctly receive signals from the base station.

III. Performance Evaluation

In this section, we will show the derivation process of performance indexes considered in this paper.

A. Obstructing Probability

Recall that the coverage of each obstacle is assumed to be a circle with a radius, r_{ca}, and that it will block all transmission paths within this range. We also assume that the coordinates of a transmitter, $\mathbf{Ts}_i$, a receiver, $\mathbf{Rc}_j$, and an obstacle, Θ^k_{OB}, are $(x^i_{\mathrm{tr}}, y^i_{\mathrm{tr}})$, $(x^j_{\mathrm{rc}}, y^j_{\mathrm{rc}})$ and $(x^k_{\mathrm{ob}}, y^k_{\mathrm{ob}})$, respectively. In addition, SBSs, relays, UEs, and obstacles are assumed to be randomly located on a plane, $\mathbb{R}_{\mathrm{P}}$, with i.i.d. uniform distributions. We assume that $\mathbb{R}_{\mathrm{P}}$ is a square area, i.e., $L_{\mathrm{P}} = W_{\mathrm{P}}$. Then $x^i_{\mathrm{tr}}, y^i_{\mathrm{tr}}, x^j_{\mathrm{rc}}, y^j_{\mathrm{rc}}, x^k_{\mathrm{ob}}, y^k_{\mathrm{ob}}$ become i.i.d. random variables that are uniformly distributed in $[-\frac{L_{\mathrm{P}}}{2}, \frac{L_{\mathrm{P}}}{2}]$. The coverage range of Θ^k_{OB} can be expressed as; $(x - x^k_{\mathrm{ob}})^2 + (y - y^k_{\mathrm{ob}})^2 \leq r^2_{\mathrm{ca}}$. By assuming $x^i_{\mathrm{tr}} > x^j_{\mathrm{rc}}$, the line segment passing through $\mathbf{Ts}_i$ and $\mathbf{Rc}_j$ is represented by

$$\frac{y - y^j_{\mathrm{rc}}}{y^i_{\mathrm{tr}} - y^j_{\mathrm{rc}}} = \frac{x - x^j_{\mathrm{rc}}}{x^i_{\mathrm{tr}} - x^j_{\mathrm{rc}}}, \quad x^j_{\mathrm{rc}} < x < x^i_{\mathrm{tr}}. \tag{25}$$

Here we define the obstructing probability by the probability that a LoS path between $\mathbf{Ts}_i$ and $\mathbf{Rc}_j$ is blocked by Θ^k_{OB}. Therefore, the obstructing probability can be expressed by

$$P_{\mathrm{OB}} = \Pr\left(\mathcal{B}^2_{\mathrm{ed}} - 4\mathcal{A}_{\mathrm{ed}}\mathcal{C}_{\mathrm{ed}} > 0\right) \times \Pr\left(x^j_{\mathrm{rc}} < x^k_{\mathrm{ob}} < x^i_{\mathrm{tr}}\right), \tag{26}$$

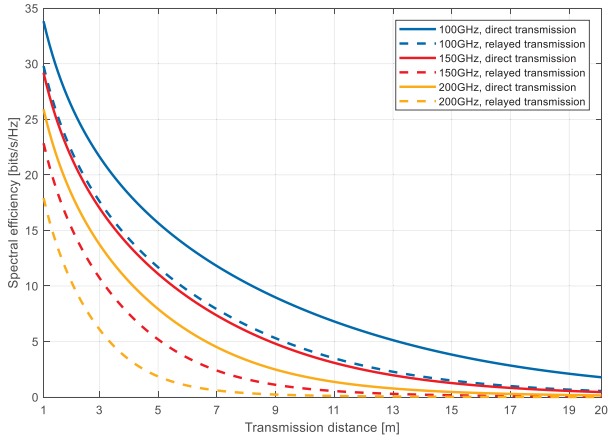

Fig. 6. Spectral efficiency versus transmission distance and frequency.

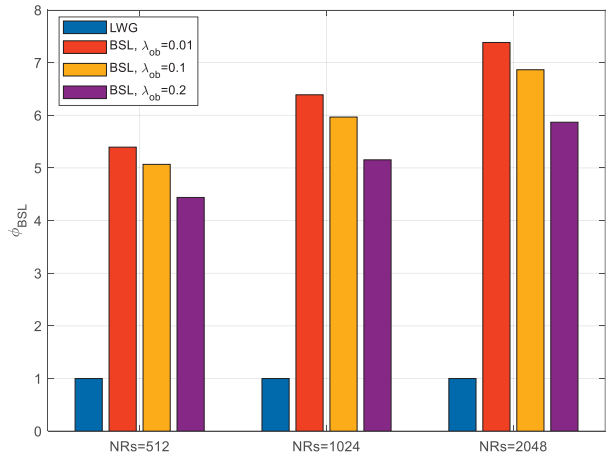

Fig. 7. ϕ_{BSL} versus codebook scale and obstacle density.

where

$$\begin{cases} \mathcal{A}_{\mathrm{ed}} = \left(\frac{y_{\mathrm{tr}}^i - y_{\mathrm{rc}}^j}{x_{\mathrm{tr}}^i - x_{\mathrm{rc}}^j}\right)^2 + 1 \\ \mathcal{B}_{\mathrm{ed}} = 2\left(x_{\mathrm{rc}}^j + x_{\mathrm{ob}}^k - \frac{\left(y_{\mathrm{rc}}^j - y_{\mathrm{ob}}^k\right)\left(y_{\mathrm{tr}}^i - y_{\mathrm{rc}}^j\right)}{x_{\mathrm{tr}}^i - x_{\mathrm{rc}}^j}\right) \\ \mathcal{C}_{\mathrm{ed}} = \left(\frac{x_{\mathrm{rc}}^j\left(y_{\mathrm{tr}}^i - y_{\mathrm{rc}}^j\right)}{x_{\mathrm{tr}}^i - x_{\mathrm{rc}}^j}\right)^2 + \left(x_{\mathrm{ob}}^k\right)^2 \\ \qquad - \frac{2x_{\mathrm{rc}}^j\left(y_{\mathrm{rc}}^j - y_{\mathrm{ob}}^k\right)\left(y_{\mathrm{tr}}^i - y_{\mathrm{rc}}^j\right)}{x_{\mathrm{tr}}^i - x_{\mathrm{rc}}^j} \\ \qquad + \left(y_{\mathrm{rc}}^j - y_{\mathrm{ob}}^k\right)^2 - r_{\mathrm{ca}}^2 \end{cases}, \tag{27}$$

B. Blocking Probability

In this paper,blocking probability is defined as the probability that there is no LoS path or relay path between the SBS Θ_{SB} and the UE Θ_{UE}. In this case,transmission between Θ_{SB} and Θ_{UE} will fail. Since the location of each SBS, relay, UE, and obstacle is i.i.d., the obstructing probability of each LoS path is also i.i.d. Thus, the probability that no LoS path exists between Θ_{SB} and Θ_{UE} can be expressed by

$$P_{\mathrm{DR}} = 1 - \left(1 - P_{\mathrm{OB}}\right)^{N_{\mathrm{ob}}}. \tag{28}$$

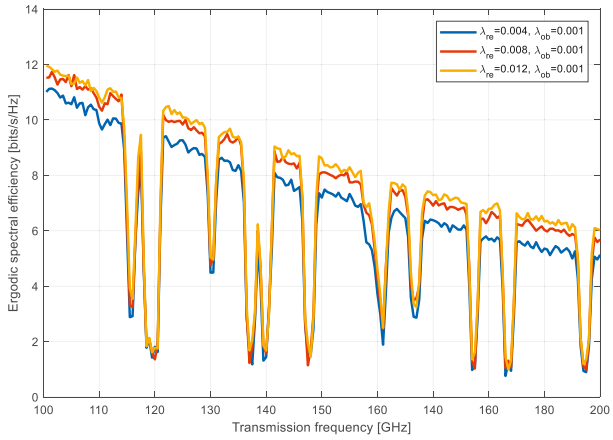

Fig. 8. Ergodic spectral efficiency versus transmission frequency and Relay density.

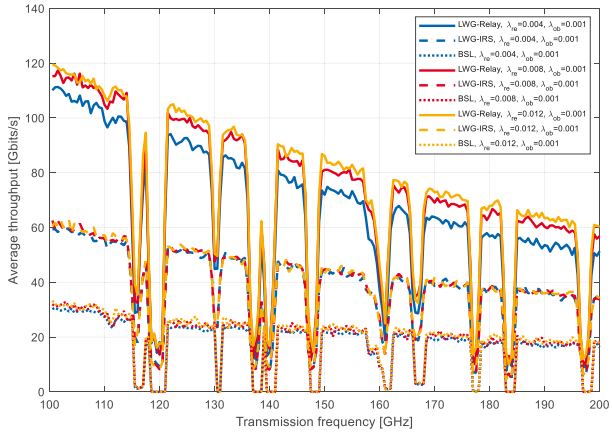

Fig. 9. Throughput versus transmission frequency and density of relays.

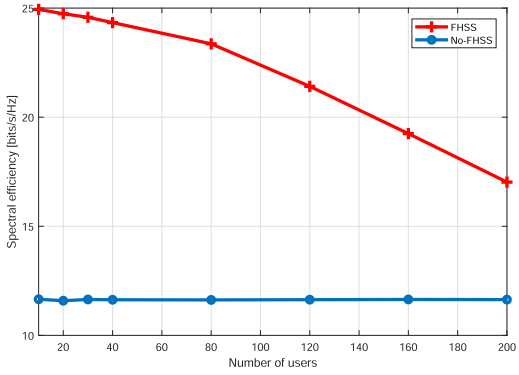

Fig. 10. Ergodic spectral efficiency versus the number of users.

The probability that norelayed path exists between Θ_{SB} and Θ_{UE} can be expressed by

$$P_{\mathrm{RE}} = \left(1 - \left(\left(1 - P_{\mathrm{OB}}\right)^{N_{\mathrm{ob}}}\right)^2\right)^{N_{\mathrm{re}}}. \tag{29}$$

TABLE I
VALUES OF SYMBOLS USED IN SIMULATION

Symbol	Definition/explanation	Value
L_{P}	Length of $\mathbb{R}_{\mathrm{P}}$	50 m
W_{P}	Width of $\mathbb{R}_{\mathrm{P}}$	50 m
P_{TR}	Transmit power	0.1 W
$\mathcal{P}$	Pressure of the environment	1 atm
$\mathcal{T}$	Temperature of the environment	296 K
$\mathcal{P}_0$	Standard pressure value	1 atm
$\mathcal{T}_{\mathrm{STP}}$	Standard temperature value	273.15 K
N_{A}	Avogadro constant	6.0221×10^{23} molecule/mol
$\mathcal{R}_{\mathrm{C}}$	Gas constant	8.2051×10^{-5} $\mathrm{m}^3 \cdot \mathrm{atm/K/mol}$
H_{PL}	Planck constant	6.6262×10^{-34} J $\cdot$ s
k_{B}	Boltzmann constant	1.3806×10^{-23} J/K
$\mathcal{T}_0$	Reference temperature	296.0 K
N_{TR}	Number of transmitting antennas	32×32
N_{RC}	Number of receiving antennas	6×6
G_{TR}	Antenna gain of transmitter	60 dB
G_{AR}	Antenna gain of receiver	20 dB
NRs	Number of codewords in $\mathbf{CB}_{\mathrm{S}}$	2048
N_{DS}	Number of data streams contained in $\mathbf{s}$	10
ΔT_{L}	Duration of the time slot	2 ns
ξ_{L}	Duration coefficient of beam discovery phase	0.5

So the blocking probability can be represented by,

$$P_{\mathrm{BL}} = P_{\mathrm{DR}} P_{\mathrm{RE}} = \left(1 - (1 - P_{\mathrm{OB}})^{N_{\mathrm{ob}}}\right) \times \left(1 - \left((1 - P_{\mathrm{OB}})^{N_{\mathrm{ob}}}\right)^2\right)^{N_{\mathrm{re}}}. \tag{30}$$

C. Ergodic Spectral Efficiency

In this paper, ergodic spectral efficiency is defined as the spectral efficiency when blocking probability is considered. Based on (17) and (28), the ergodic spectral efficiency when a LoS path exists between Θ_{SB} and Θ_{UE} can be expressed by (31).

$$\begin{aligned} C_{\mathrm{egd}} &= (1 - P_{\mathrm{DR}})\, \mathbb{E}\left(C_{\mathrm{AD}}\right) \\ &= (1 - P_{\mathrm{DR}})\, \mathbb{E}\left(\log_2 \det\left(\mathbf{I}_{N_{\mathrm{RC}}} + \frac{P_{\mathrm{TR}}}{\sigma_{\mathrm{s}}^2} \mathbf{H} \mathbf{F}_{\mathrm{CB}}^{*} (\mathbf{F}_{\mathrm{CB}}^{*})^H \mathbf{H}^H\right)\right) \end{aligned} \tag{31}$$

Based on (20) and (29), the ergodic spectral efficiency when a relayed path exists between Θ_{SB} and Θ_{UE} can be expressed by (32).

$$\begin{aligned} C_{\mathrm{egr}} &= (1 - P_{\mathrm{DR}})\, \mathbb{E}\left(C_{\mathrm{AR}}\right) \\ &= (1 - P_{\mathrm{DR}})\, \mathbb{E}\left(\log_2 \det\left(\mathbf{I}_{N_{\mathrm{DS}}} + \frac{P_{\mathrm{TR}}}{N_{\mathrm{DS}}} \mathbf{H}_{\mathrm{RE}} \mathbf{F}_{\mathrm{RB}}^{*} \mathbf{R}_{\mathrm{n}}^{-1} \mathbf{W}_{\mathrm{RE}}^{H} \mathbf{H} \mathbf{F}_{\mathrm{CB}}^{*} (\mathbf{F}_{\mathrm{CB}}^{*})^H \right.\right. \\ &\quad \left.\left. \times\ \mathbf{H}^H \mathbf{W}_{\mathrm{RE}} (\mathbf{F}_{\mathrm{RB}}^{*})^H \mathbf{H}_{\mathrm{RE}}^{H}\right)\right) \end{aligned} \tag{32}$$

Since the direct path between Θ_{SB} and Θ_{UE} has priority over the relayed path, the ergodic spectral efficiency can be represented by,

$$\begin{aligned} C_{\mathrm{EG}} = {} & (1 - P_{\mathrm{DR}})\, \mathbb{E}\left(C_{\mathrm{AD}}\right) \\ & + P_{\mathrm{DR}} (1 - P_{\mathrm{DR}})\, \mathbb{E}\left(C_{\mathrm{AR}}\right) \end{aligned} \tag{33}$$

D. Average Throughput

In this paper, a time slot ΔT_{L} is divided into two phases, beam discovery and data transmission. The duration of the former, which is based the LWG-based method, is defined as $\Delta T_{\mathrm{LB}} = \xi_{\mathrm{L}} \Delta T_{\mathrm{L}}$, where $0 < \xi_{\mathrm{L}} < 1$. For the data transmission phase, the duration is defined by $\Delta T_{\mathrm{LD}} = (1 - \xi_{\mathrm{L}}) \Delta T_{\mathrm{L}}$. Obviously, we have $\Delta T_{\mathrm{L}} = \Delta T_{\mathrm{LB}} + \Delta T_{\mathrm{LD}}$, and the average throughput of the network during K_{TS} time slots can be shown as,

$$Tr_{\mathrm{LW}} = \frac{1}{K_{\mathrm{TS}} \Delta T_{\mathrm{L}}} \sum_{k=1}^{K_{\mathrm{TS}}} B_{\mathrm{AV}} C_{\mathrm{EG}} \left(1 - \xi_{\mathrm{L}}\right) \Delta T_{\mathrm{L}} \tag{34}$$

where B_{AV} is the available bandwidth for data transmission, where

$$B_{\mathrm{AV}} = B_{\mathrm{T}} \Pr\left(\alpha_{\mathrm{PL}}\left(f, \mathcal{R}\right) \leq \lambda_{\mathrm{PL}}\right), \tag{35}$$

where B_{T} is the total bandwidth used for data transmission and λ_{PL} is the threshold of the path loss.

IV. SIMULATION RESULTS

The values of the parameters used in our simulations are shown in Table I. The density of relays and obstacles are defined by $\lambda_{\mathrm{re}} = N_{\mathrm{re}}/(L_{\mathrm{P}} W_{\mathrm{P}})$ and $\lambda_{\mathrm{ob}} = N_{\mathrm{ob}}/(L_{\mathrm{P}} W_{\mathrm{P}})$, respectively. For the sake of comparison,we choose the LWG and intelligent reflecting surface (IRS) assisted network to make the comparison. Configurations of the IRS can be found in [31], [49]. Also, the IEEE 802.11ad is chosen as the baseline (BSL) algorithm. Notice that LWG is also used for beam discovery of LWG-IRS assisted networks, so the time spent on one attempt for beam discovery is the same as for LWG-Relay assisted network and LWG-IRS assisted networks. Here we define the time spent on one attempt for beam discovery of these methods (i.e., LWG-Relay assisted, LWG-IRS assisted, and the BSL) as; $\Delta T_{\mathrm{BSB}} = \Delta T_{\mathrm{LB}} = \xi_{\mathrm{L}} \Delta T_{\mathrm{L}}$. Also, the time spent on the data transmission phase for these three methods is set at; $\Delta T_{\mathrm{BSD}} = \Delta T_{\mathrm{LD}} = (1 - \xi_{\mathrm{L}}) \Delta T_{\mathrm{L}}$. For the BSL andLWG-Relay/IRS-assisted methods, the time spent on beam discovery before the data transmission phase is defined by T_{BSB}

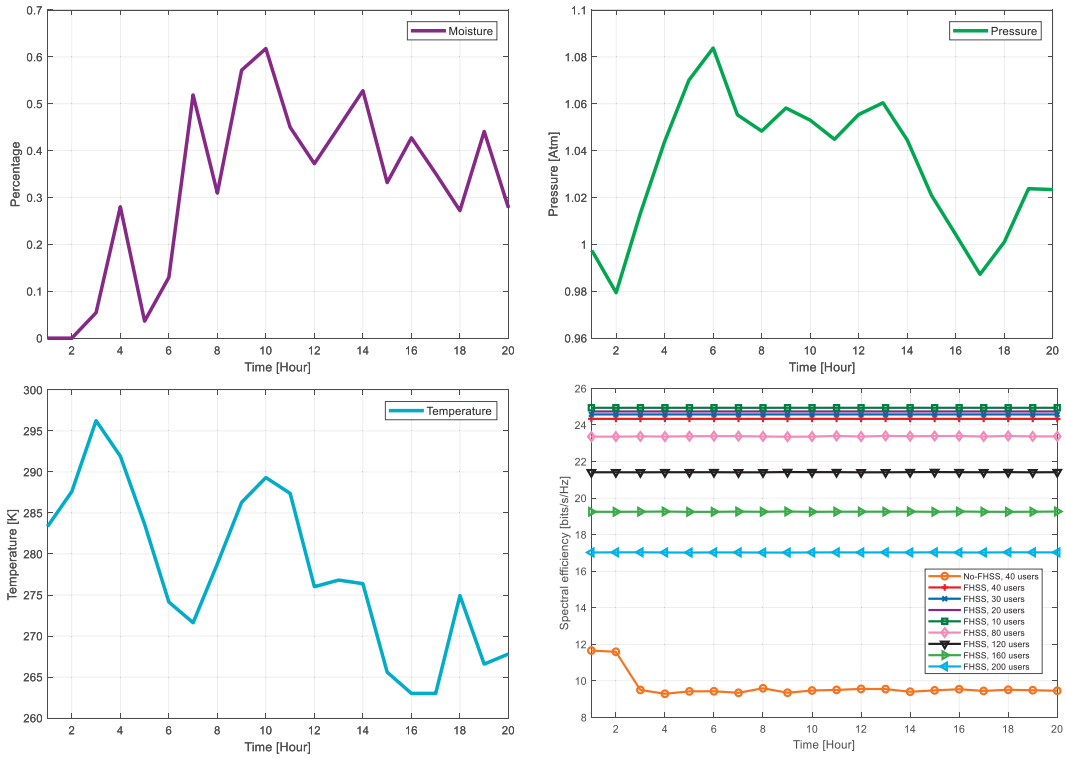

Fig. 11. Ergodic spectral efficiency versus the number of users and time.

and T_{LWB}, respectively. Then, the normalized time spent on beam discovery before a data transmission phase can be defined by $\phi_{\mathrm{BSL}} = \frac{T_{\mathrm{BSB}}}{T_{\mathrm{LWB}}}$. Also, as an example, large antenna arrays with 1024 antenna units are adopted by the transmitters to generate pencil-like beams to compensate the high path loss on sub-THz bands.

The spectral efficiencies C_{AD} and C_{AR} in (17) and (20), versus transmission distance, with respect to the transmission frequency, are shown in Fig. 6. As can be expected, C_{AD} and C_{AR} decrease significantly as $R_{i,j}$ increases. For a fixed $R_{i,j}$, the values of C_{AD} and C_{AR} decrease at a higher transmission frequency. Such a decrease in C_{AD} and C_{AR} could be attributed to the relationship between transmission distance, frequency, and path loss, which is represented in (2). When the transmission distance and frequency are both fixed, the values of C_{AD} and C_{AR} for relayed transmission are lower than those of direct transmission. This is because the amplification effect of the relay is not large enough to compensate for the extra path loss when the relay is used.

The simulation results of normalized time spent on beam discovery before a data transmission phase, ϕ_{BSL}, versus obstacle density, with respect to the scale of the codebook NRs and different beam discovery methods, are shown in Fig. 7. The simulation result marked by LWG in the figure is the throughput of our proposed methodand those marked by BSL are the simulation results corresponding to the baseline method. As we can see, the value of ϕ_{BSL} increases at higher NRs. This is because the BSL method will require more time onbeam discovery when there are more sectors that need to be swept. For a given NRs, the value of ϕ_{BSL} decreases at a higher obstacle density, λ_{ob} as direct or relayed transmission paths will be blocked by more obstacles. Then, when there is no feasible transmission path between the SBS and UE, the BSL method will stop the beam sweeping process instead of sweeping all the sectors.Our proposed LWG-assisted method can do beam discovery with one single shot.

The simulation results of ergodic spectral efficiency C_{EG} in (33), versus transmission frequency, with respect to the density of relays, are presented in Fig. 8. Since we consider the block effect caused by obstacles, the ergodic spectral efficiency C_{EG} is lower than C_{AD} and C_{AR} presented in Fig. 6, for a given transmission frequency. When the transmission frequency is fixed, the value of C_{EG} rises as the relay density, N_{re}, increases. This is because a higher density of relays may shorten the distance between the transmitters and receivers, hence further reducing the impact of the path loss $\alpha_{\mathrm{PL}}(f, \mathcal{R})$.

The simulation results of average throughput, Tr_{LW}, versus transmission frequency, with respect to the density of relays, are shown in Fig. 9 for three methods, i.e., LWG-Relay assisted, LWG-IRS assisted, and BSL. The bandwidth for data transmission is configured within ± 10 GHz of the transmission frequency. Also, the impact of the availability of the bandwidth, i.e., B_{AV}, is considered. As can be clearly observed from this figure, the throughput performance of our proposed method is far superior to that of the baseline method. This is because we use a codebook that can form a high narrow beam at Sub-THz/THz resulting in a higher antenna gain. Therefore, the baseline algorithm needs to spend a great deal of time on sector sweeping, and only a small amount of time can be used for data transmission. In addition, we can observe that when

λ_{re} is greater than 0.008, increasing λ_{re} does not significantly improve throughput performance. This result indicates that the optimal density of λ_{re} should consider the value of λ_{ob} and the size of the area. Also, the proposed LWG-Relay assisted method has a higher performance than the LWG-IRS assisted method. This is mainly because the simulation area in this paper is as large as $2500\,\mathrm{m}^2$. The passive beamforming performed by the IRS can not provide enough antenna gain to compensate for the high path loss at the sub-THz band within such a large area.

In our simulation,BPSK modulation is adoptedand the symbol error caused by low SNR is considered. In Figs. 10 and 11, a spectrum from 0.12 THz to 0.14 THz is split into 400 frequency bands, each with 50 MHz bandwidth. According to the feedback from LWG, users will perform low frequency hopping (1000 symbols per hop) on the frequency bands whose channel conditions have been least affected by frequency selective attenuations. For example, in the case of 200 users, the 200 channels with the smallest attenuation are selected.Under these conditions, the corresponding hopping rate is 50 K hops per second. Assuming that the clock drift of all components was randomly distributed within 50 parts per million (ppm), the clock offset between UEs and the base station in one hop period will be bounded within 2 ns. Conversely, in non-FHSS methods users are randomly assigned to different frequency bands. When using frequency bands with high attenuations, the users' performance will be significantly degraded.

The environmental parameters, including moisture, pressure and temperature are varying with time. In Fig. 11, these environmental parameters are displayed at a rate of one point per hour. It can be observed that this is a set of slow-changing parameters. In our simulation, the base station will periodically update the channel map according tofeedback from the LWG receiver every 10 seconds. It is shown that channel conditionsare mainly affected by moisture; the higher the moisture, the worse the channel condition and the less spectrum efficiency. As shown in this figure, the non-FHSS mode is sensitive to environmental parameters, but the FHSS mode is robust tovarying environmental parameters when using frequency bands with low attenuation

V. Conclusion

This paper mainly focuses on beam discovery, precoding, and combining issues for sub-THz communications. The main challenge is how to deal with channel characteristics, precoding complexities,existence of obstacles, and atmospheric attenuation, which can allgreatly impact the communication performance at Sub-THz and THz bands. In this paper an LWG-assisted high-resolution codebook based method is proposed. This method aims to effectively reduce the duration of the beam discovery phase, as well as the complexity ofhybrid precoding. Moreover, to support the proposed method, an empirical data based channel model is adopted for the sub-THz band.To prevent transmission at vulnerable frequencies, wepropose FHSS where the carrier frequency of the transmit signal hops among multiple discrete carrier frequencies. The simulation results verify that our method is capable of achievinghigher throughput performancesas compared with the sector sweeping based method, e.g., IEEE 802.11ad.

References

[1] Z. Chen et al., "A survey on terahertz communications," *China Commun.*, vol. 16, no. 2, pp. 1–35, Feb. 2019.

[2] L. You, X. Gao, G. Y. Li, X. Xia, and N. Ma, "BDMA for millimeter-wave/terahertz massive MIMO transmission with per-beam synchronization," *IEEE J. Sel. Areas Commun.*, vol. 35, no. 7, pp. 1550–1563, Jul. 2017.

[3] J. Seungyong et al., "Broadly tunable monolithic room-temperature terahertz quantum cascade laser sources," *Nature Commun.*, vol. 5, no. 1, pp. 1–7, 2014.

[4] Q. Y. Lu et al., "Widely tuned room temperature terahertz quantum cascade laser sources based on difference-frequency generation," *Appl. Phys. Lett.*, vol. 101, no. 25, 2012, Art. no. 251121.

[5] H. Song and T. Nagatsuma, "Present and future of terahertz communications," *IEEE Trans. Terahertz Sci. Technol.*, vol. 1, no. 1, pp. 256–263, Sep. 2011.

[6] Y. Xiaohu et al., "Towards 6G wireless communication networks: Vision, enabling technologies, and new paradigm shifts," *Sc. China Inf. Sci.*, vol. 64, no. 1, pp. 1–74, 2021.

[7] I. F. Akyildiz and J. M. Jornet, "Realizing ultra-massive MIMO (1024x1024) communication in the (0.06C10) terahertz band," *Nano Commun. Netw.*, vol. 8, pp. 46–54, 2016.

[8] H. Sarieddeen, M.-S. Alouini, and T. Y. Al-Naffouri, "An overview of signal processing techniques for terahertz communications," *Proc. IEEE*, vol. 109, no. 10, pp. 1628–1665, Oct. 2021.

[9] J. Tan and L. Dai, "THz precoding for 6G: Challenges, solutions, and opportunities," *IEEE Wireless Commun.*, early access, May 9, 2022, doi: 10.1109/MWC.015.2100674.

[10] L. Yan, C. Han, and J. Yuan, "A dynamic array-of-subarrays architecture and hybrid precoding algorithms for terahertz wireless communications," *IEEE J. Sel. Areas Commun.*, vol. 38, no. 9, pp. 2041–2056, Sep. 2020.

[11] J. Tan and L. Dai, "Delay-phase precoding for THz massive MIMO with beam split," *Proc. IEEE Glob. Commun. Conf.*, Waikoloa, HI, USA, 2019, pp. 1–6.

[12] R. Zhang, W. Hao, G. Sun, and S. Yang, "Hybrid precoding design for wideband THz massive MIMO-OFDM systems with beam squint," *IEEE Syst. J.*, vol. 15, no. 3, pp. 3925–3928, Sep. 2021.

[13] S. A. Busari, K. M. S. Huq, S. Mumtaz, and J. Rodriguez, "Terahertz massive MIMO for beyond-5G wireless communication," in *Proc. IEEE Int. Conf. Commun.*, Shanghai, China, 2019, pp. 1–6.

[14] D. Li, D. Qiao, L. Zhang, and G. Y. Li, "Performance analysis of indoor THz communications with one-bit precoding," in *Proc. IEEE Glob. Commun. Conf.*, Abu Dhabi, United Arab Emirates, 2018, pp. 1–7.

[15] B. Peng, S. Wesemann, K. Guan, W. Templ, and T. Krner, "Precoding and detection for broadband single carrier terahertz massive MIMO systems using LSQR algorithm," *IEEE Trans. Wireless Commun.*, vol. 18, no. 2, pp. 1026–1040, Feb. 2019.

[16] H. Yuan, N. Yang, K. Yang, C. Han, and J. An, "Enabling massive connections using hybrid beamforming in terahertz micro-scale networks," in *Proc. IEEE Wireless Commun. Netw. Conf.*, Seoul, South Korea, 2020, pp. 1–7.

[17] H. Zhang, H. Zhang, W. Liu, K. Long, J. Dong, and V. C. M. Leung, "Energy efficient user clustering, hybrid precoding and power optimization in terahertz MIMO-NOMA systems," *IEEE J. Sel. Areas Commun.*, vol. 38, no. 9, pp. 2074–2085, Sep. 2020.

[18] S. A. Busari et al., "Generalized hybrid beamforming for vehicular connectivity using THz massive MIMO," *IEEE Trans. Veh. Technol.*, vol. 68, no. 9, pp. 8372–8383, Sep. 2019.

[19] H. Yuan, N. Yang, K. Yang, C. Han, and J. An, "Hybrid beamforming for terahertz multi-carrier systems over frequency selective fading," *IEEE Trans. Commun.*, vol. 68, no. 10, pp. 6186–6199, Oct. 2020.

[20] C. Lin, G. Y. Li, and L. Wang, "Subarray-based coordinated beamforming training for mmWave and Sub-THz communications," *IEEE J. Sel. Areas Commun.*, vol. 35, no. 9, pp. 2115–2126, Sep. 2017.

[21] Z. Zhong and H. Gharavi, "Spectral and energy efficiencies of millimeter wave MIMO with configurable hybrid precoding," *IEEE Trans. Veh. Technol.*, vol. 68, no. 6, pp. 5732–5746, Jun. 2019.

[22] C. Cheng, S. Kim, and A. Zajic, "Comparison of path loss models for indoor 30 GHz, 140 GHz, and 300 GHz channels," in *Proc. 11th Eur. Conf. Antennas Propag.*, Paris, France, 2017, pp. 716–720.
[23] K. M. S. Huq, S. A. Busari, J. Rodriguez, V. Frascolla, W. Bazzi, and D. C. Sicker, "Terahertz-enabled wireless system for beyond-5G ultra-fast networks: A brief survey," *IEEE Netw.*, vol. 33, no. 4, pp. 89–95, Jul./Aug. 2019.
[24] I. F. Akyildiz, C. Han, and S. Nie, "Combating the distance problem in the millimeter wave and terahertz frequency bands," *IEEE Commun. Mag.*, vol. 56, no. 6, pp. 102–108, Jun. 2018.
[25] Q. Wu and R. Zhang, "Towards smart and reconfigurable environment: Intelligent reflecting surface aided wireless network," *IEEE Commun. Mag.*, vol. 58, no. 1, pp. 106–112, Jan. 2020.
[26] Q. Wu, S. Zhang, B. Zheng, C. You, and R. Zhang, "Intelligent reflecting surface aided wireless communications: A tutorial," *IEEE Trans. Commun.*, vol. 110, no. 9, pp. 1380–1400, Sep. 2022.
[27] B. Ning, Z. Chen, W. Chen, Y. Du, and J. Fang, "Terahertz multi-user massive MIMO with intelligent reflecting surface: Beam training and hybrid beamforming," *IEEE Trans. Veh. Technol.*, vol. 70, no. 2, pp. 1376–1393, Feb. 2021.
[28] M. Xinying et al., "Intelligent reflecting surface enhanced indoor terahertz communication systems," *Nano Commun. Netw.*, vol. 24, 2020, Art. no. 100284.
[29] Q. Wu and R. Zhang, "Intelligent reflecting surface enhanced wireless network via joint active and passive beamforming," *IEEE Trans. Wirel. Commun.*, vol. 18, no. 11, pp. 5394–5409, Nov. 2019.
[30] P. Yijin et al., "Sum rate maximization for intelligent reflecting surface assisted terahertz communications," 2020, *arXiv:2008.12246*.
[31] X. Ma et al., "Joint channel estimation and data rate maximization for intelligent reflecting surface assisted terahertz MIMO communication systems," *IEEE Access*, vol. 8, pp. 99565–99581, 2020.
[32] E. Bjornson, O. Ozdogan, and E. G. Larsson, "Intelligent reflecting surface versus decode-and-forward: How large surfaces are needed to beat relaying ?," *IEEE Wireless Commun. Lett.*, vol. 9, no. 2, pp. 244–248, Feb. 2020.
[33] Z. Miao, Z. Hao, B. Jin, and Z. N. Chen, "Low-Profile 2–D THz Airy Beam Generator Using the Phase-Only Reflective Metasurface," *IEEE Trans. Antennas Propag.*, vol. 68, no. 3, pp. 1503–1513, Mar. 2020.
[34] H. Jalili and O. Momeni, "A 0.34–THz Wideband Wide–Angle 2–D Steering Phased Array in 0.13–μm SiGe BiCMOS," *IEEE J. Solid–State Circuits*, vol. 54, no. 9, pp. 2449–2461, Sep. 2019.
[35] Y. Ghasempour et al., "Single-shot link discovery for terahertz wireless networks," *Nature Commun.*, vol. 11, no. 1, pp. 1–6, 2020.
[36] N. J. Karl, R. W. McKinney, Y. Monnai, R. Mendis, and D. M. Mittleman, "Frequency-division multiplexing in the terahertz range using a leaky-wave antenna," *Nature Photon.*, vol. 9, pp. 717–720, Sep. 2015.
[37] H. Guerboukha et al., "Efficient leaky-wave antennas at terahertz frequencies generating highly directional beams," *Appl. Phys. Lett.*, vol. 117, no. 26, Aug. 2020, Art. no. 261103.
[38] J. M. Jornet and I. F. Akyildiz, "Channel modeling and capacity analysis for electromagnetic wireless nanonetworks in the terahertz band," *IEEE Trans. Wireless Commun.*, vol. 10, no. 10, pp. 3211–3221, Oct. 2011.
[39] J. Ye and H. Gharavi, "Attractor selection based limited feedback hybrid precoding for uplink V2I communications," *IEEE Trans. Veh. Technol.*, vol. 69, no. 4, pp. 3943–3953, Apr. 2020.
[40] C. Lin and G. Y. Li, "Energy-efficient design of indoor mmWave and Sub-THz systems with antenna arrays," *IEEE Trans. Wireless Commun.*, vol. 15, no. 7, pp. 4660–4672, Jul. 2016.
[41] J. F. Federici, J. Ma, and L. Moeller, "Review of weather impact on outdoor terahertz wireless communication links," *Nano Commun. Netw.*, vol. 10, pp. 13–26, 2016.
[42] J. H. Van Vleck and V. F. Weisskopf, "On the shape of collision broadened lines," *Rev. Mod. Phys.*, vol. 17, no. 2–3, pp. 227–236, Apr. 1945.
[43] W. Wu, D. Liu, Z. Li, X. Hou, and M. Liu, "Two-stage 3D codebook design and beam training for millimeter-wave massive MIMO systems," in *Proc. IEEE 85th Veh. Technol. Conf.*, 2017, pp. 1–7.
[44] L. Jiang and H. Jafarkhani, "mmWave amplify-and-forward MIMO relay networks with hybrid precoding/combining design," *IEEE Trans. Wirel. Commun.*, vol. 19, no. 2, pp. 1333–1346, Feb. 2020.
[45] O. E. Ayach, S. Rajagopal, S. Abu-Surra, Z. Pi, and R. W. Heath, "Spatially sparse precoding in millimeter wave MIMO systems," *IEEE Trans. Wireless Commun.*, vol. 13, no. 3, pp. 1499–1513, Mar. 2014.
[46] Q. Xia, Z. Hossain, M. Medley, and J. M. Jornet, "A link-layer synchronization and medium access control protocol for terahertz-band communication networks," *IEEE Trans. Mobile Comput.*, vol. 20, no. 1, pp. 2–18, Jan. 2021.
[47] *IEEE Standard for a Precision Clock Synchronization Protocol for Networked Measurement and Control Systems*, IEEE Standard 1588–2002, 2002.
[48] B. Hu and H. Gharavi, "A hybrid wired/wireless deterministic network for smart grid," *IEEE Wireless Commun.*, vol. 28, no. 3, pp. 138–143, Jun. 2021.
[49] W. Hao et al., "Robust design for intelligent reflecting surface-assisted MIMO-OFDMA terahertz IoT networks," *IEEE Internet Things J.*, vol. 8, no. 16, pp. 13052–13064, Aug. 2021.

Junliang Ye (Member, IEEE) received the B.Sc. degree in communication engineering from the China University of Geosciences, Wuhan, China, in 2011, and the Ph.D. degree from the Huazhong University of Science and Technology, Wuhan, in 2018. He is currently a Guest Researcher with the National Institute of Standards and Technology, U.S. Department of Commerce, Gaithersburg, MD, USA. His research interests include heterogeneous networks, stochastic geometry, mobility-based access models of cellular networks, millimeter wave communications, and next-generation wireless communication.

Hamid Gharavi (Life Fellow, IEEE) received the Ph.D. degree from Loughborough University, Loughborough, UK, in 1980. In 1982, he joined the Visual Communication Research Department, AT & T, Bell Laboratories, Holmdel, NJ, USA. He was then transferred to Bell Communications Research (Bellcore) after the AT & T-Bell divestiture, where he became a consultant on video technology and a Distinguished Member of Research Staff. In 1993, he joined Loughborough University as a Professor and the Chair of communication engineering. Since September 1998, he has been with the National Institute of Standards and Technology, Gaithersburg, MD, USA. He was a core Member of Study Group XV (Specialist Group on Coding for Visual Telephony) of the International Communications Standardization Body CCITT (ITU-T) and a Member of the IEEE 2030 standard working group. His research interests include smart grid, wireless multimedia, mobile communications and wireless systems, mobile ad hoc networks, and visual communications. He was the recipient of the Charles Babbage Premium Award from the Institute of Electronics and Radio Engineering in 1986, and IEEE CAS Society Darlington Best Paper Award in 1989, and Washington Academy of Science Distinguished Career in Science Award for 2017. He was a Distinguished Lecturer of the IEEE Communication Society. He has been the Guest Editor of a number of special issues of the Proceedings of the IEEE, including *Smart Grid*, *Sensor Networks & Applications*, *Wireless Multimedia Communications*, *Advanced Automobile Technologies*, and Grid Resilience. He was the TPC Co-Chair of IEEE SmartGridComm in 2010 and 2012. He was a Member of the Editorial Board of Proceedings of the IEEE from January 2003 to December 2008. He was the Editor-in-Chief of IEEE TRANSACTIONS ON CAS FOR VIDEO TECHNOLOGY and IEEE WIRELESS COMMUNICATIONS.

Bin Hu (Senior Member, IEEE) received the Ph.D. degree from the School of Electronics and Computer science, University of Southampton, Southampton, U.K., in 2006. Since September 2006, he has been with the National Institute of Standards and Technology, U.S. Department of Commerce, Gaithersburg, MD, USA, where he is currently a Research Scientist in advanced network technologies division. His research interests include wireless communication, video/image transmission, smart grid, deterministic networks, and mobile ad-hoc networks.